Preparation of Bone Powder for FTIR-ATR Analysis: The Particle Size Effect

Ioannis Kontopoulos[1], Samantha Presslee[1], Kirsty Penkman[1, 2], and Matthew J. Collins[1, 3]

1. BioArCh, Department of Archaeology, University of York, United Kingdom
2. BioArCh, Department of Chemistry, University of York, United Kingdom
3. Natural History Museum, University of Copenhagen, Denmark

Abstract

Fourier transform infrared (FTIR) spectroscopy using attenuated total reflection (ATR) is commonly used for the examination of bone. During sample preparation bone is commonly ground, changing the particle size distribution. Although previous studies have examined changes in crystallinity caused by the intensity of grinding using FTIR, the effect of sample preparation (i.e. particle size and bone tissue type) on the FTIR data is still unknown.

This study reports on the bone powder particle size effects on mid-IR spectra and within sample variation (i.e. periosteal, mesosteal, trabecular) using FTIR-ATR. Twenty-four archaeological human and faunal bone samples (5 heated and 19 unheated) of different chronological age (Neolithic to post-Medieval) and origin (Belgium, Britain, Denmark, Greece) were ground using either (1) a ball-mill grinder, or (2) an agate pestle and mortar, and split into grain fractions (>500 μm, 250-500 μm, 125-250 μm, 63-125 μm, and 20-63 μm).

Bone powder particle size has a strong but predictable effect on the infrared splitting factor (IRSF), carbonate/phosphate (C/P) ratio, and amide/phosphate (Am/P) values. The absorbance and positions of the main peaks, the 2nd derivative components of the phosphate and carbonate bands, as well as the full width at half maximum (FWHM) of the 1010 cm^{-1} phosphate peak are particle size dependent. This is likely to be because of the impact of the particle size on the short- and long-range crystal order, as well as the contact between the sample and the prism, and hence the penetration depth of the IR light. Variations can be also observed between periosteal, cortical and trabecular areas of bone. We therefore propose a standard preparation method for bone powder for FTIR-ATR analysis that significantly improves accuracy, consistency, reliability, replicability and comparability of the data, enabling systematic evaluation of bone in archaeological, anthropological, paleontological, forensic and biomedical studies.

Keywords: Bone; FTIR-ATR; sample preparation; particle size; bioapatite; crystal order/disorder

1. Introduction

Bone is a complex inorganic/organic composite material with a hierarchical structural order that is reflected in its biomechanical properties [1–7]. Biological apatite (BAp) nanocrystals are carbonated calcium phosphate mineral compounds with species, age, or pathology related compositional/structural variation generally represented by the formula (Ca^{2+}, Na^{+}, Mg^{2+}, [])$_{10}$ (PO_4^{3-}, HPO_4^{3-}, CO_3^{2-})$_6$ (OH^{-}, F^{-}, Cl^{-}, CO_3^{2-}, O, [])$_2$ [4,8–14]. BAp dominates bone (i.e. 65-70 wt. %), with the organic content (primarily collagen type I) accounting for 20-25 wt. % and the remaining 5-10 wt. % being water [2].

The information that can be preserved within skeletal tissues has shaped the way we interpret the past [15,16]. However, in archaeological and fossil bone, diagenesis leads to its partial or complete destruction, with accompanying loss of vital biochemical information [17–21]. Over the past decades, Fourier transform infrared (FTIR) spectroscopy has been increasingly used to better understand bone diagenesis, as well as for screening of archaeological and fossil bone [22–34]. The correspondence between measurements taken with transmission FTIR, ATR (attenuated total reflection) and DRIFT (diffuse reflectance infrared Fourier transform) can be problematic [34–36]. Nevertheless, because FTIR is so minimally invasive/destructive and provides information on both the inorganic and organic structures present, it has been commonly used to assess the postmortem changes in BAp crystals (e.g. crystallinity, carbonate to phosphate content, fluorine and calcite content), and the organic preservation in heated, unheated and pathological bones [25,31,35,37–44].

The infrared splitting factor (IRSF, also termed crystallinity) is assumed to be related to the crystal order and size of bone mineral [2,25,45–47] which can change *in vivo* (ontogenetic bone growth/maturity) and post-mortem (diagenesis, heating) [e.g. 8,22,48,49]. Higher crystallinity is considered to be an indication of an increase in BAp crystals' size and atomic order due to either: a) a growth of the larger crystals at the expense of the smaller ones (i.e. Ostwald ripening); b) a loss of the smaller crystals; or c) both. Lower IRSF values reflect the smaller size and higher atomic disorder of the BAp crystals [2,22,25,26,29,46,47,50].

These changes in bioapatite characteristics are caused by several ionic substitutions that take place both in the hydrated layer and the apatite core, and strongly affect its dissolution/recrystallization behaviour [4,51]. Carbonate (CO_3^{2-}) content (c. 4-6 wt. %), which is considered to be related to crystallinity (and thus IRSF), is such an example of ionic substitution of carbonate for phosphate (type B), and vice versa, in the bioapatite structure [4,25,52–58]. Although type A substitution (CO_3^{2-} for OH^{-}) might be relatively limited in BAp, its role should not be neglected [4,25,31,56,57,59]. FTIR has also been used to assess organic preservation in archaeological and fossil bone using the Am/P (amide to phosphate) ratio [e.g. 29,60], while other minor ionic concentrations of elements (such as Mg, Na, Sr, K, Zn and F) also play a special role in its structure and function [4,11,53–55,61,62].

Although the contribution of FTIR to the study of archaeological and fossil bone is indisputable, the usefulness of the indices (such as IRSF) as a measure of BAp preservation and change has been questioned [26,31,48,58,63,64]. The introduction of the relatively new FTIR-ATR technique offers rapid, cost efficient and minimally destructive analysis [30,34,49], but the issues of accuracy, precision, reproducibility and comparability of the data have not yet been resolved [36,48].

Past studies have tried to tackle these issues by investigating the effect of sample preparation methods on bone IRSF values, with a decrease in IRSF reported with more intensive pulverization [26]. Surovell & Stiner [26] argue that grinding may actually introduce variations in crystallinity that may mask the original signal due to structural changes caused to the BAp crystals. They propose two possibilities that could explain the phenomenon: a) changes are primarily caused by the particle separation of bone mineral of differing crystallinity (i.e. separation hypothesis), or b) grinding affects the bioapatite crystal structure (i.e. destruction hypothesis), and subsequently, the mid-IR spectra. Overall, it has been argued that there seems to be a destruction of BAp crystals during grinding, although when there is no control, or grinding is excessive, it is difficult to differentiate between the actual bone crystallinity from that introduced during sample preparation [26]. Hollund et al. [34] also observed significant preparation-based differences (i.e. drilling and grinding with and without sieving) between IRSF, C/P and Am/P values. The grinding effect was more evident in samples of higher crystallinity, so Hollund et al. [34] proposed drilling bone without sieving as an alternative to the Surovell and Stiner [26] preparation method.

Repeated grinding of calcite during preparation for FTIR measurements has been shown to affect the material's atomic order as revealed by changes in the mid-IR spectrum [65,66]. Asscher et al. [46,47] tried to explore the effects of grinding on bone and tooth, and decouple it from the atomic disorder effect to better assess the preservation state of archaeological/fossil bone. They compared the IRSF values of samples repeatedly ground for variable amounts of time and plotted them against the full width at half maximum (FWHM) of the main v_3 phosphate peak in mid-IR spectra (i.e. 1010 cm^{-1}). From the relationship observed, it was shown that grinding (i.e. particle size) affects both the short (IRSF) and long (FWHM at 1010 cm^{-1}) range order of bone. Thus, the use of the grinding curve approach can significantly increase the sensitivity of FTIR for monitoring diagenesis (slopes of the grinding curves increase with poorer preservation), as compared to the IRSF alone, and it can also allow the identification of differences in crystal size/atomic order of different animal species and hard tissues (bone, dentine and enamel mineral) [46].

While this trendline method partly shows the importance of particle size (still uncontrolled) on the mid-IR spectrum, it requires regrinding and measuring the same sample repeatedly for several times. Furthermore, the powders were analysed in KBr pellets, requiring significant amounts of material mixed with KBr. Excessive grinding can also lead to a contamination of bone powder or even damage surviving biomolecules in samples that could be also used for DNA or protein analysis [e.g. 67,68], making FTIR

KBr and grinding curves a destructive method and wasting precious material, in lieu of additional information on crystalline order.

Therefore, although previous studies have recommended optimal methods, the precise effects of particle size on FTIR data has never been thoroughly explored, and only in a limited number of studies particles have been homogeneous [25–27,36]. Excluding the variations due to sample preparation methods that are related with the atomic order/disorder, small but insignificant tissue specific variations have also been reported for both unheated [27] and heated bone [48].

The increased adoption of FTIR-ATR further changes the equation. The method is being increasingly commonly used because it is a cost efficient, rapid and minimally destructive method, and has the potential to act as screening method to determine which bones show optimal preservation. The powder can be extracted for biomolecules after analysis with no loss of material. This study presents the effects of sample selection (i.e. periosteal, mesosteal, trabecular bone) as well as particle size on the mid-IR spectrum of bone measured by FTIR-ATR. We propose a standard preparation procedure for the analysis of bone powder using FTIR-ATR to improve data accuracy, precision, comparability and reproducibility. The process focuses on the particle size effect and requires bone powder of even sized particles. This approach improves the contact between the sample and the prism, allows a deeper penetration depth of the IR radiation into individual BAp crystals, and avoids damage in the short- and long-range order of bioapatite crystals by using optimal bone powder particle sizes.

2. Materials and Methods

Twenty-four archaeological human and animal bone samples (5 heated and 19 unheated) of different chronological age (Neolithic to post-Medieval) and origin (Belgium, Britain, Denmark, Greece) were used in this study (Table S1 - supplementary material). Prior to analysis, the trabecular, periosteal/sub-periosteal and endosteal/sub-endosteal tissues were mechanically removed using a scalpel. For the examination of the particle size effect on mid-IR spectra, the mesosteal (mid-cortical) tissue of nineteen specimens was ground using either (1) a Retsch oscillating steel ball mill grinder at 20 Hz for 20-25 seconds x 3-5 times, or (2) an agate pestle and mortar.

Samples were sieved using Endecotts woven stainless steel mesh sieves with an aperture size of 500 μm, 250 μm, 125 μm, 63 μm, and 20 μm to produce 5 particle size classes (i.e. > 500 μm, 250-500 μm, 125-250 μm, 63-125 μm, 20-63 μm). Six of the archaeological samples (3 fauna, 2 heated and 1 unheated human) were also ground down to c. 1 μm using a Retsch PM100 ball mill grinder. The container, lid and ball grinders were cooled using liquid nitrogen to reduce potential destruction of crystals due to heat produced during the grinding process. One subsample from each of the six samples was ground for 3 minutes at 400 rpm twice, the container being cooled in liquid nitrogen in between each

run, while a second subsample was ground at 600 rpm for 5 minutes. Particle size of the subsamples was compared to other previously measured microground samples under the microscope and were shown to be of similar size, i.e. c. 1 μm. Samples were split into three different groups (i.e. fauna, unheated human and heated human specimens) to allow the observation of any differences that might be related to the pre-burial histories of bones (e.g. cooking, boiling), preservation state and animal species related BAp crystal order/disorder.

Bone powder of 20-63 μm particle size from the periosteal, mesosteal and trabecular tissues of 5 human samples was also analyzed by FTIR-ATR (Table S2 - supplementary material). Additionally, bone powder from two modern human mesosteal samples (particle size 20-63 μm), one modern bovine (particle size from >500 μm to 20-63 μm) and synthetic hydroxyapatite (HAp) (particle size from >500 μm to 20-63 μm) were used as references (see Table S3 - supplementary material).

FTIR measurements were performed in triplicate for each sample on each different particle size powder fraction using an Alpha Platinum FTIR-ATR spectrometer (range: 4000-400 cm^{-1}; no. of scans: 144; zero-filling factor: 4; resolution: 4 cm^{-1}; mode: absorbance). About 2-3 mg of bone powder were put on the optic window with a diamond crystal. For good contact with uniform pressure between the crystal and the sample, the pressure of the applicator was controlled using the pressure control spot. After each measurement, the crystal plate and the anvil of the pressure applicator were thoroughly cleaned using isopropyl alcohol. Spectra were analysed using OPUS 7.5 software.

Infrared splitting factor (IRSF) was assessed after Weiner and Bar-Yosef [22], carbonate-to-phosphate (C/P) ratio was calculated as in Wright and Schwarcz [25], type B carbonate substitutions relative to phosphate (BPI) was estimated as in Sponheimer and Lee-Thorp [38], and amide-to-phosphate (Am/P) was assessed according to Trueman et al. [29]. All indices were estimated after baseline correction (Figure 1; Box 1).

The full width at half maximum (FWHM) of the c. 1010 cm^{-1} peak was measured after baseline subtraction to assess the atomic order/disorder of the samples [9,46,47]. The 2nd derivatives were produced to explore the overlapping bands at the v_4, v_3, v_1 PO_4^{3-} and v_2 CO_3^{2-} bands using the OriginPro 2017 and the Savitzky-Golay filter with 9 smoothing points and a polynomial order of 4. Statistical analysis carried out using IBM SPSS v.24 and the significance level was set at $p = 0.05$.

Box 1. Indices - Baseline correction

1. Infrared splitting factor (IRSF) was assessed using the equation introduced by Weiner and Bar-Yosef [26] that measures the heights at c. 600 cm^{-1} + c. 560 cm^{-1}, divided by the trough between them at c. 590 cm^{-1}, using a baseline correction from the c. 400-420 cm^{-1} to the c.

630-670 cm^{-1} troughs (Figure 1a). The two peaks are characteristic of the v_4 antisymmetric bending mode of orthophosphate ion [49].

$$\mathrm{IRSF} = \frac{600\ \mathrm{cm^{-1}} + 560\ \mathrm{cm^{-1}}}{590\ \mathrm{cm^{-1}}}$$

2. Carbonate-to-phosphate (C/P) ratio was estimated as in Wright and Schwarcz [29] by dividing the main v_3 carbonate peak height at c. 1410 cm^{-1} with the main v_3 phosphate vibrational band at c. 1010 cm^{-1} [29]. The baseline correction was drawn from c. 1590 cm^{-1} to c. 1290 cm^{-1} and from c. 1150-1180 cm^{-1} to c. 880-900 cm^{-1}, respectively (Figure 1b and Figure 1c).

$$\mathrm{C/P} = \frac{1410\ \mathrm{cm^{-1}}}{1010\ \mathrm{cm^{-1}}}$$

3. The type B carbonate substitutions relative to phosphate (BPI) were calculated from the ratio of the peak heights at c. 1410 cm^{-1} and c. 600 cm^{-1} as in Sponheimer and Lee-Thorp [42] using the same baselines for both peaks as above (Figure 1a and Figure 1c).

$$\mathrm{BPI} = \frac{1410\ \mathrm{cm^{-1}}}{600\ \mathrm{cm^{-1}}}$$

4. Amide-to-phosphate (Am/P) was assessed by the v_1 amide at c. 1640 cm^{-1} divided by the main v_3 phosphate peak at c. 1010 cm^{-1} [33]. Baseline correction was from c. 1720 cm^{-1} to c. 1590 cm^{-1} and c. 1150 cm^{-1} to c. 890 cm^{-1}, respectively (Figure 1b and Figure 1d).

$$\mathrm{Am/P} = \frac{1640\ \mathrm{cm^{-1}}}{1010\ \mathrm{cm^{-1}}}$$

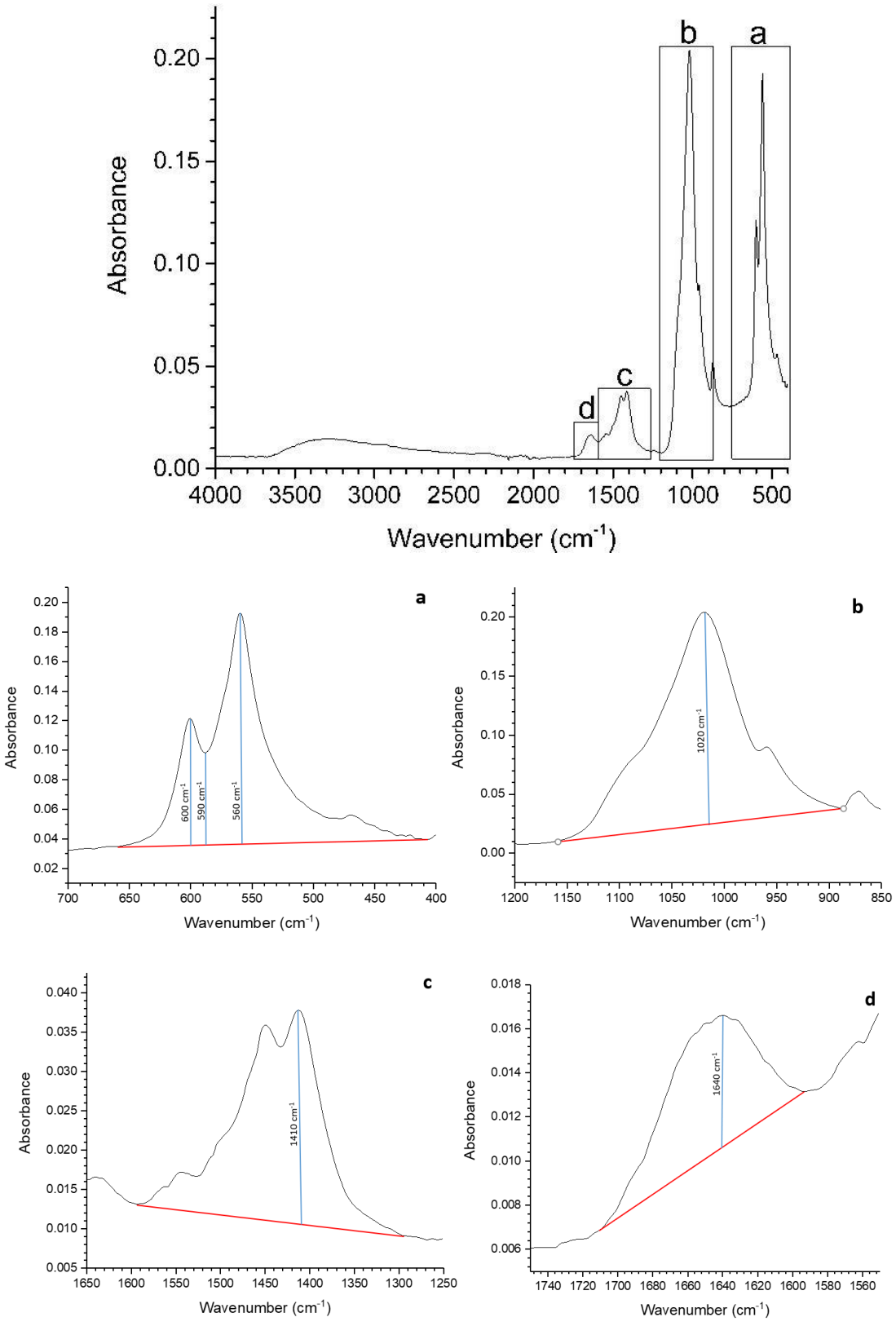

Figure 1. The mid-IR spectra of 20-63 µm particle size archaeological human mesosteal bone powder (MEC77). The spectral bands used for IRSF (a), C/P (b, c), and Am/P (b, d) are highlighted. Figures 1a-d display the peak positions (blue lines) for IRSF, C/P and Am/P indices as well as the baselines (red lines).

3. Results and Discussion

3.1. Tissue-specific variations

Within-sample variations can be observed in crystallinity, carbonate and organic content of the different bone tissue areas (Figure 2 and Table S4 - supplementary material), although there is no statistically significant difference between periosteal, mesosteal and trabecular bone tissue for either IRSF (x^2=1.680, p= 0.432), C/P (x^2=0.306, p= 0.858) or Am/P (x^2=3.847, p= 0.146). IRSF values in the periosteal tissue appear lower compared to the mesosteal and trabecular tissues (Figure 2a), carbonate content displays no observable pattern (Figure 2b), whereas Am/P values appear higher in the periosteal tissue (Figure 2c).

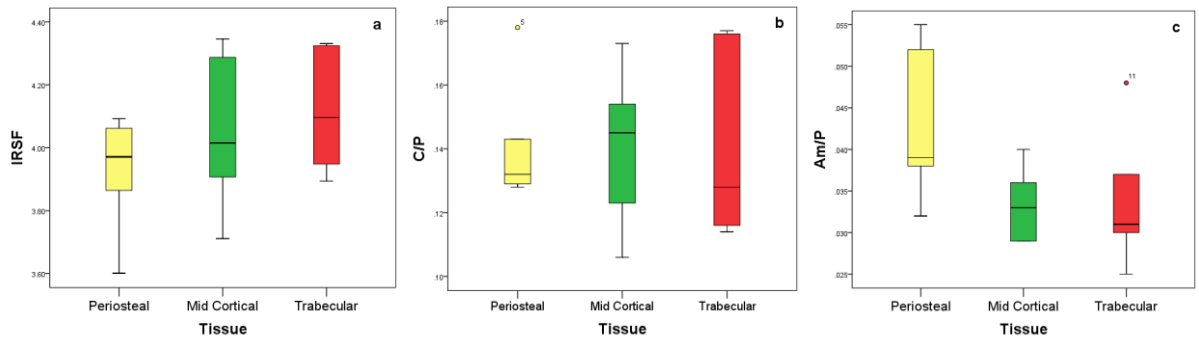

Figure 2. Box plots showing the IRSF (a), C/P (b) and Am/P (c) indices in the periosteal, mid cortical (mesosteal) and trabecular tissues. Notice the lower IRSF (a) and C/P (b) values in the periosteal tissue.

The organization of bone and the conditions of the depositional micro-environment (e.g. local hydrology, pH, depth) may strongly affect BAp structural characteristics, composition and their dissolution/recrystallization rate [5,6,8,60,69–71]. In modern human bone, a gradient from the osteon outwards (tissue specific, age-related variations) has been previously observed by Paschalis et al. [8], with the areas farther from the haversian canal displaying increased crystallinity, higher type B carbonate and lower type A carbonate content. A small variation in carbonate content within trabecular bone tissue (i.e. center to edges gradient) has also been reported by Ou-Yang et al. [72].

In archaeological and fossil bone, when an equilibrium between bone and its burial environment is reached and dissolution/recrystallization slows down, any change in the conditions would result in re-equilibration between the bone chemistry and its surroundings [51,71]. With respect to that behaviour, Stiner et al. [23] have observed that the outer surfaces of modern bone which had been exposed for 2 and 9 years post-mortem in Israel and New Mexico (USA), respectively, displayed higher crystallinity than the inner cortical areas. In a similar attempt to record mineralogical and compositional changes in bones of large mammals exposed on the ground surface in Amboseli National Park (Kenya) for up to 26 years, Trueman et al. [29] also observed that the crystallinity in the periosteal surfaces was higher than

in the other bone tissue areas (inner cortical) as early as 2 years post-mortem. The higher periosteal IRSF values were accompanied by higher concentrations of rare earth elements (e.g. Ba and La) which also showed a gradual decrease towards the inner cortex [29]. When the cortical bone was compared with trabecular bone in the Middle Palaeolithic Hayonim cave (Israel) the IRSF values for spongy tissues were found slightly higher [27].

Therefore, the tissue-specific differences in crystallinity, carbonate and organic content can vary within and between sites [27,31,60], while other factors such as the post-mortem interval or the size of the bone itself can also affect its post-mortem behaviour and interaction with its depositional environment [26]. Consequently, although there is no universal pattern for tissue-specific variations found in archaeological and fossil bone, the necessity for homogenization of samples prior to analysis using FTIR-ATR through the mechanical removal of the periosteal, trabecular and endosteal bone tissues and use of the mesosteal (mid-cortical) tissue is indisputable for the improvement of accuracy, precision, reproducibility and comparability of data.

3.2. Particle size effect

3.2.1. Effects on IR indices

Bone powder particle size predictably affects the IRSF, C/P and Am/P values in all samples (Tables S3 and S5 - supplementary material). Very strong inverse relationships are observed when IRSF is plotted against C/P (Figure 3). Carbonate content strongly affects crystallinity changes as it is inversely related to crystal growth (i.e. it acts as an inhibitor) [4,11], and the very strong inverse relationship of C/P with IRSF seen in our data supports an interaction between carbonate and phosphate in BAp crystals (e.g. [25]). A very strong correlation is also observed between these two indices and the samples' particle size (Figure 3).

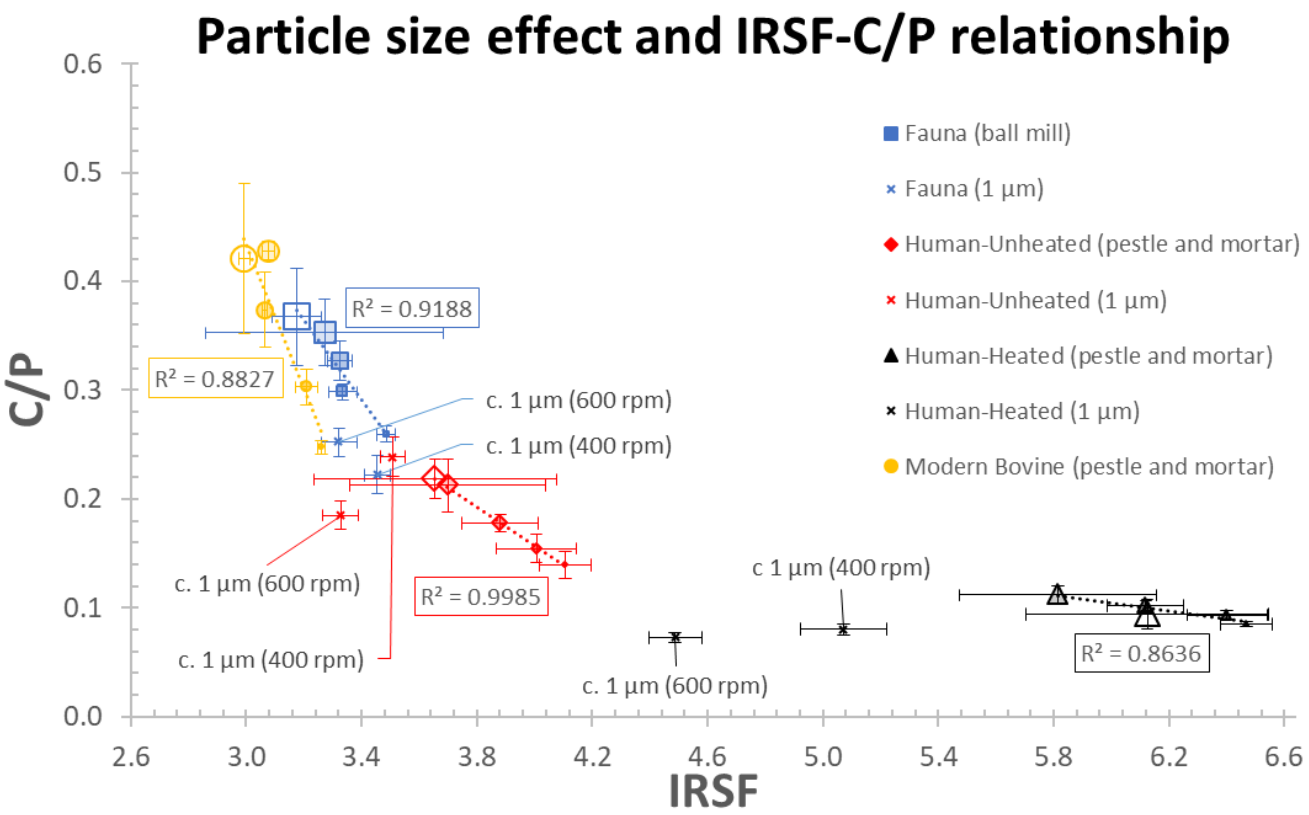

Figure 3. IRSF-C/P relationship with the samples' particle size in modern and archaeological bone. Datapoint markers' sizes gradually decrease with decreasing particle size (i.e. **>500 µm**: size 10, 100% transparent; **250-500 µm**: size 8, 80% transparent; **125-250 µm**: size 6, 60% transparent; **63-125 µm**: size 4, 40% transparent; **20-63 µm**: size 2, 20% transparent). Error bars represent estimated standard deviations.

Faunal bones (n=9) display a very strong relationship between particle size and mid-IR indices that reflect crystal composition (Figure 3; Fig.S1 - supplementary material). IRSF, C/P and Am/P demonstrate statistically significant differences for particle sizes ranging from >500 µm to 20-63 µm (IRSF: x^2= 20.809, p= 0.000; C/P: x^2= 13.910, p= 0.008; Am/P: x^2= 10.783, p= 0.029). IRSF gradually increases with decreasing particle size and drops at the 1 µm powder (Figure 3; Fig.S1a - supplementary material). On the contrary, C/P gradually decreases with decreasing particle size, except for the 1 µm at 600 rpm that increases to the 20-63 µm levels (Figure 3; Fig.S1b - supplementary material). Am/P gradually decreases with decreasing particle size and stabilises at the 1 µm particle size (Fig.S1c - supplementary material). Additionally, at the 1 µm size the samples' powder colour becomes dark grey/blackish.

The unheated human samples' (n=5) IRSF and C/P values also display statistically significant differences between the different particle sizes (x^2= 16.903, p= 0.002) and (x^2= 17.853, p= 0.001), respectively. Specifically, there is a gradual increase in IRSF and a gradual decrease in C/P with decreasing particle size (Figure 3; Fig.S2a and S2b - supplementary material). On the other hand, while Am/P shows almost no statistically significant differences (x^2= 9.343, p= 0.053), a similar general pattern can be observed, with a gradual decrease in Am/P values with decreasing particle size; the exception is

the 250-500 μm that displays an increase in both C/P and Am/P (Fig.S2b and S2c - supplementary material). In particle sizes of c. 1 μm, IRSF significantly drops for both the 400 rpm and 600 rpm preparation methods (Fig.S2a - supplementary material). However, C/P and Am/P are increased at 400 rpm (similar values to the >500 μm powder) but decreased when prepared at 600 rpm (similar values to the 125-250 μm powder) (Fig.S2b and S2c - supplementary material). A similar discoloration (dark grey/blackish) of the samples' powder is also observed at the 1 μm level.

In contrast, in the heated human samples, there is no statistically significant difference between different particle sizes (>500 μm to 20-63 μm) and any of the indices [IRSF: (x^2=2.267, p=0.687); C/P: (x^2=3.244, p=0.518)]; Am/P: (x^2=2.722, p=0.605)]. Not surprisingly, however, a pattern can be observed for crystallinity, with an overall increase in IRSF that is accompanied by a decrease in C/P with decreasing particle size (Fig.S3a and S3b - supplementary material). For particle sizes of about 1 μm, there seems to be a rapid decrease in IRSF and a more gentle drop in C/P values (Fig.S3a and S3b - supplementary material). With regard to the reference samples, modern bovine bone shows similar relationships to the archaeological fauna and human unheated specimens, while synthetic HAp displays a decrease in IRSF values with decreasing particle size (Figure 3; Fig.S4 and Table S5 - supplementary material).

The effect of particle size distribution and shape on IR spectra has been previously reported by Kristova et al. [73], and it is assumed to be primarily because of the better packing and higher surface area of the samples consisting of smaller particles [74]. In our samples, the smaller the particle size, the higher the crystallinity and the lower the carbonate content; this could be simply assumed to be because of the better contact between the sample and the prism, and the deeper penetration depth of the IR radiation into individual BAp crystals [74]. The exposure of a larger amount of BAp crystals to the IR radiation in samples consisting of smaller particle size powders also results in more accurate, precise and reproducible data. On the other hand, the coarser the sample, the poorer the contact between the sample and the prism due to increased void spaces (i.e. porosity) in the sample [74].

Breaking the crystal-crystal interaction (i.e. crystal fusion) may also contribute to the phenomenon observed in our data [11]. While it is still poorly understood as a process, the interaction between the crystals' hydrated layers (i.e. amorphous hydrophilic surface layers) in bone has been proposed as a possible explanation for the binding between the BAp crystals, pulled together by van der Waals forces [75,76]. As BAp crystals are often seen as aggregate clusters in transmission electron microscopy (TEM) (e.g. [29]), this supports a "separation hypothesis" up to the 20-63 μm level, as grinding could simply divide and expose some of the merged BAp crystals which have amalgamated to form larger crystals (i.e. Ostwald ripening).

It is, therefore, likely that the initial small size of the BAp crystals (i.e. about 30 nm long x 20 nm wide x 2-4 nm thick) [1,2] makes their destruction difficult during grinding when bone powder particle size

remains over 20 µm [11], even when the BAp crystals further increase in size due to diagenesis (e.g. [31] estimated that for IRSF between 3.0-3.9, the average maximum BAp crystal length would be about 65 nm). Hence the Surovell and Stiner [26] "destruction hypothesis" (i.e. grinding damages the BAp crystal structure) seems rather unlikely for unheated modern and archaeological bone with over 20 µm bone powder particle size. However, the large drop in IRSF values observed at the 1 µm level is probably an indication that the BAp crystals are distorted by some breaking during grinding at a critical point between 1 µm and 20 µm, leading again to a more disordered (short-range) crystal state and a more variable particle size distribution that affects the penetration depth and accuracy of data [77].

3.2.2. Effects on IR absorbance

A very strong relationship between IR absorbance at 560 cm^{-1}, 600 cm^{-1}, 1010 cm^{-1} and 1410 cm^{-1} and particle size can be observed from the peak heights after baseline correction in all samples (Figure 4 and Figure 5). Absorbance is higher when the particle size decreases, except for C/P in heated samples (due to the loss of carbonate content during heating; Figure 5). Samples also display a small average shift towards higher wavenumbers with decreasing particle size (Table S6 - supplementary material).

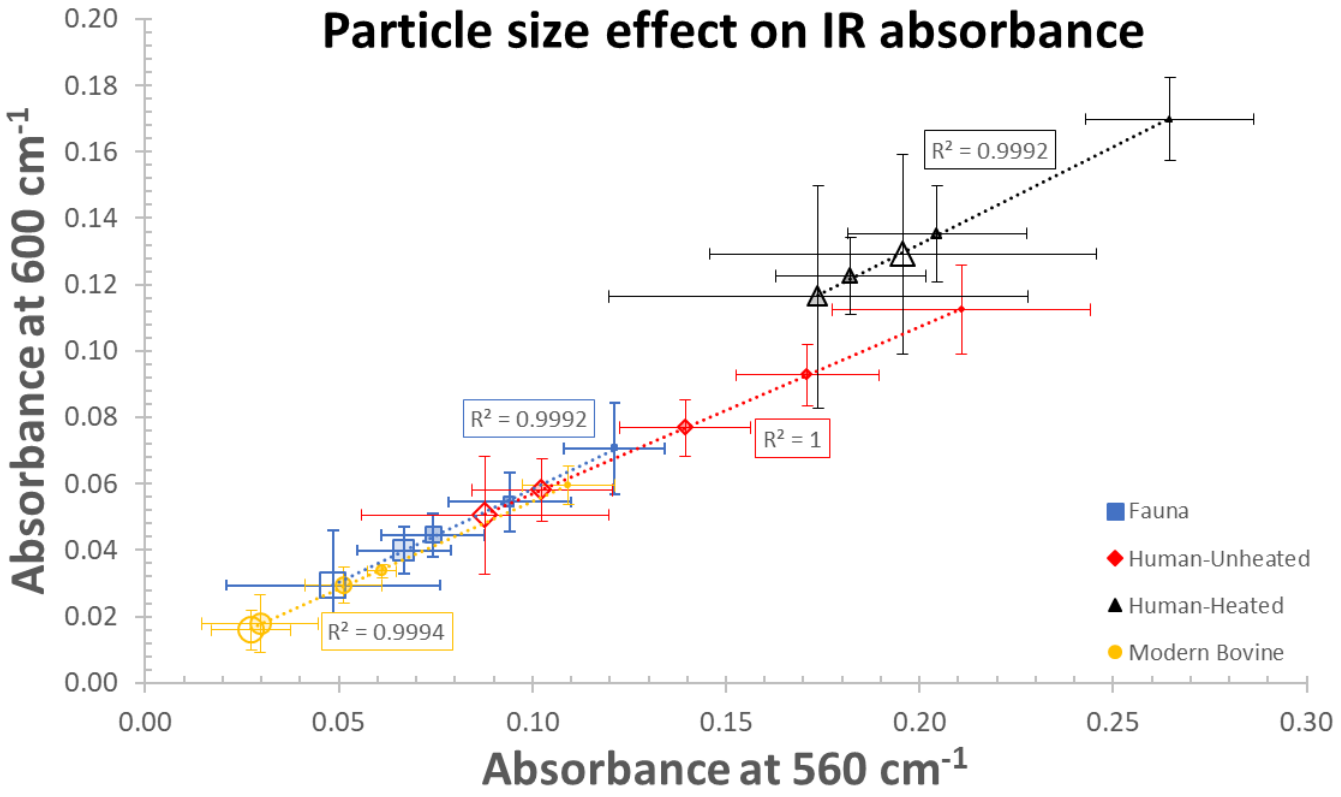

Figure 4. The particle size effect on the absorbance of IR of the main v_4 phosphate peaks at 560 cm^{-1} and 600 cm^{-1}. Markers and error bars as in **Figure 3**.

The absorbance of the IR radiation in our samples exhibited a very strong linear relationship with particle size, with the smaller the particle size, the higher the absorbance. This further supports the effectiveness of the 20-63 µm particle size powders compared to coarser samples. The only exception was the

absorbance at the c. 1410 cm^{-1} peak for the heated human samples, due to the prior loss of most of their carbonate content during heating. Such an effect of particle size on the intensity and region of IR bands of minerals has been reported in past studies [e.g. 65,66,74], with the smaller the particle size, the higher the absorbance of IR and the narrower the bandwidth. Although the penetration depth of the IR light for diamond ATR crystals has been found to correlate with grinding [78], the IR penetration depths (i.e. full effective path length) and absorbance may sometimes vary due to scattering, interference and refractive index of the crystal (i.e. diamond vs Ge) [74].

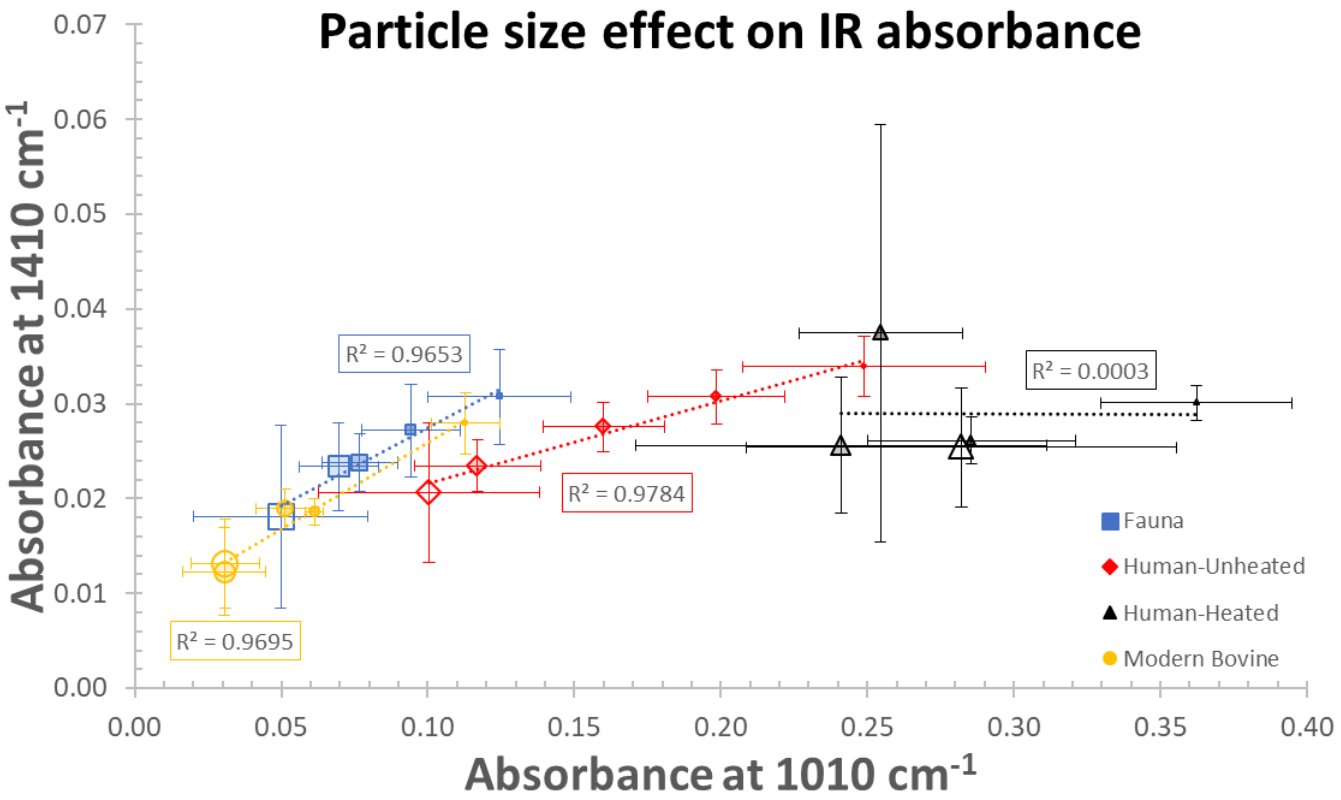

Figure 5. The particle size effect on the absorbance of IR of the main v_3 phosphate peak at 1010 cm^{-1} and the main v_3 carbonate peak at 1410 cm^{-1}. Markers and error bars as in **Figure 3**.

3.2.3. Effects on BAp order/disorder

The FWHM at 1010 cm^{-1} is considered to reflect the long-range order of a crystal (higher FWHM values indicate higher long-range disorder), hence the homogeneity between the different clusters of atoms arranged in a predictable pattern [4,50]. IRSF reflects the short-range order (higher IRSF values indicate higher short-range order) which is affected by the ionic substitutions in neighbouring atoms [38]. In this study, the FWHM of the 1010 cm^{-1} main phosphate peak is strongly related with crystallinity and particle size (>500 to 20-63 μm) with three main patterns being identified (Figure 6). The first is observed in modern bovine bone, exhibiting a rapid decrease in FWHM with decreasing particle size but a small increase in IRSF values, similar to the pattern seen in the well-preserved archaeological bovine specimen SAR38. The second pattern is that observed in the poorly preserved PRO8 (archaeological

bovine) and MEC77 (archaeological human) samples, which demonstrate slightly different trendlines with the increase in crystallinity accompanying the decrease in FWHM being higher. Finally, the third pattern (i.e. heated archaeological human bone and synthetic HAp) is characterised by a much flatter trendline, resulting from a smaller decrease in FWHM and a stronger IRSF increase. When the particle size drops to c. 1 µm, IRSF and FWHM show no clear relationships (Figure 6).

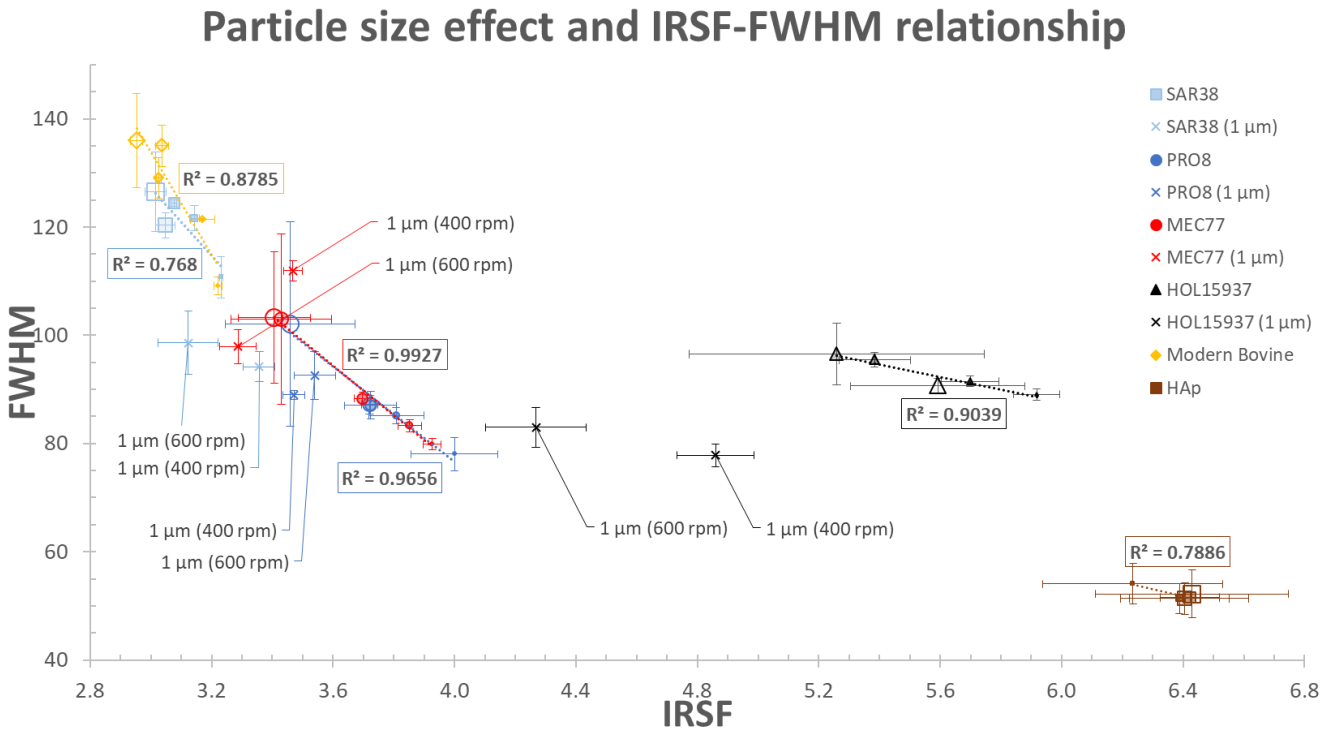

Figure 6. Graph displaying the particle size effect on the IRSF and the FWHM at 1010 cm^{-1}. Markers and error bars as in **Figure 3**.

Grinding and particle size can thus affect both IRSF and FWHM, with the different gradients of the curves reflecting the differences in BAp crystal size, and short- and long-range order of the samples associated with the particle size effect. On a similar note, synthetic HAp displays a decrease in IRSF with decreasing particle size and an almost unaltered FWHM, indicative of a fairly constant long-range order and a damage to the crystals' size and short-range order (Figure 6). Therefore, crystal distortion depends on the powder particle size and the size of the BAp crystals related to the preservation state or characteristics of each species.

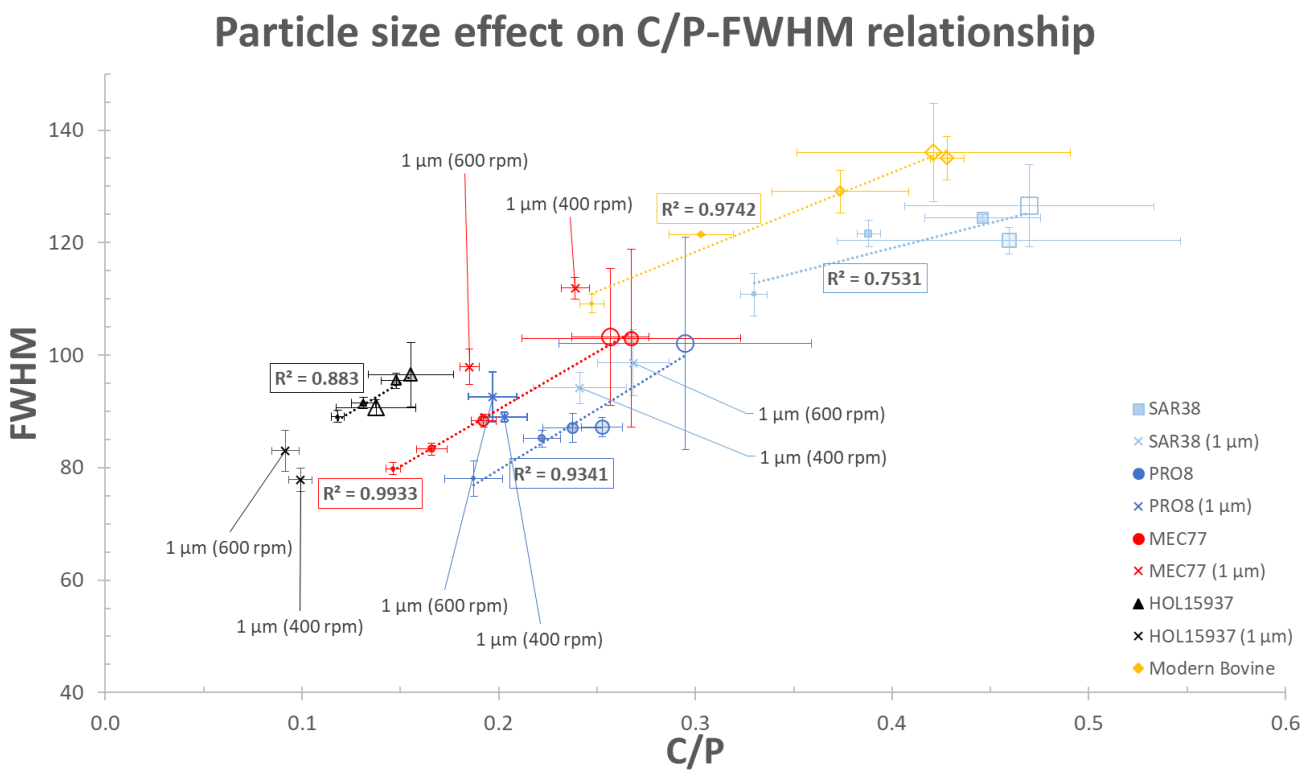

Figure 7. Graph displaying the particle size effect on the C/P and the FWHM at 1010 cm^{-1}. Markers and error bars as in **Figure 3**.

The effect of particle size on the C/P to FWHM relationship is also marked in all samples for particle sizes varying from >500 µm to 20 µm (Figure 7). As with IRSF, the same three groups can be recognised: a) the modern bovine and SAR38 having similar trend lines characterized by a decrease in carbonate content as well as in FWHM with decreasing particle size; b) PRO8 and MEC77 showing a slightly smaller drop in C/P and FWHM values; and c) the HOL15937 heated archaeological human sample that displays a lesser degree of carbonate and FWHM change due to the loss of most carbonate during heating. In samples of c. 1 µm particle size, C/P also displays no specific patterns (Figure 7).

The atomic order/disorder, the morphology and the size of the BAp crystals are highly interrelated and dependent on carbonate concentrations [4]. The very strong linear relationship of CO_3^{2-} with FWHM (Figure 7) confirms the assumptions made by other researchers (e.g. [4,11,52,53]) that, except for the effects on the crystal dimensions, the higher the carbonate content in the crystal lattice the more disordered the crystal will be. An exchange of carbonate for phosphate has been found to correlate with a change in the *a*- and *c*-axis crystal dimensions that results in more disordered crystals [52,53]. This assumption is supported by the differences in the O-O distances in PO_4^{3-} and CO_3^{2-}; thus a substitution of the smaller CO_3^{2-} by the larger PO_4^{3-} or a replacement of the larger CO_3^{2-} for the smaller OH^- would increase the unit cell dimensions [54].

The peak height at c. 1410 cm^{-1} displays a very strong linear relationship (R^2=0.96) with this at c. 872 cm^{-1}. As both peaks reflect the type B carbonate environment in bioapatite crystals [57] it corroborates LeGeros [52] account of the bone carbonate exchange that primarily occurs at the phosphate sites of the crystal lattice (i.e. type B) [4]. Type A carbonate substitutions are considered to occur at high temperatures (e.g. 900-1000^o C) with the exclusion of water, while type B CO_3^{2-} substitutions can take place at much lower temperatures (e.g. 25-100^o C) [52]. Thus, as precipitation of carbonate for phosphate (and vice versa in archaeological and fossil bone) in bone occurs at the lower temperature range, type B CO_3^{2-}, which seems to be the predominant form of carbonate in skeletal tissues, is possibly adsorbed on the surfaces of the BAp crystals (i.e. the sloping faces of the substituted phosphate ions) and not incorporated into the crystal structure [52,53,59,79,80].

The characteristic v_2 carbonate vibrations that appear at c. 871 cm^{-1} for type B, c. 878 cm^{-1} for type A1 ("stuffed") and c. 866 cm^{-1} for type A2 ("labile"-surface) CO_3^{2-} [8,56,59,80] are also observed in the 2nd derivative components of our modern bovine data from >500 μm to 63-125 μm (Figure 8). Among these components, the c. 871 cm^{-1} type B carbonate appears to be more prominent than the other two (Figure 8). The most important observation, however, is the disappearance of the c. 866 cm^{-1} peak in the 2nd derivative spectra of the modern bovine bone at the 20-63 μm particle size and its absence from all the 2nd derivative spectra of all the archaeological specimens in all particle sizes (Fig. S5-S8 - supplementary material). This observation justifies its characterization as "labile"-surface carbonate [8,56,80] and shows that a possible removal of ions (e.g. carbonate) from the crystal surface during grinding of modern bone cannot be overlooked [11]. The very strong correlation between C/P and type B CO_3^{2-} for the more degraded samples in this experiment could also be an indication of such a loss of the "labile" type A carbonate from the BAp crystal.

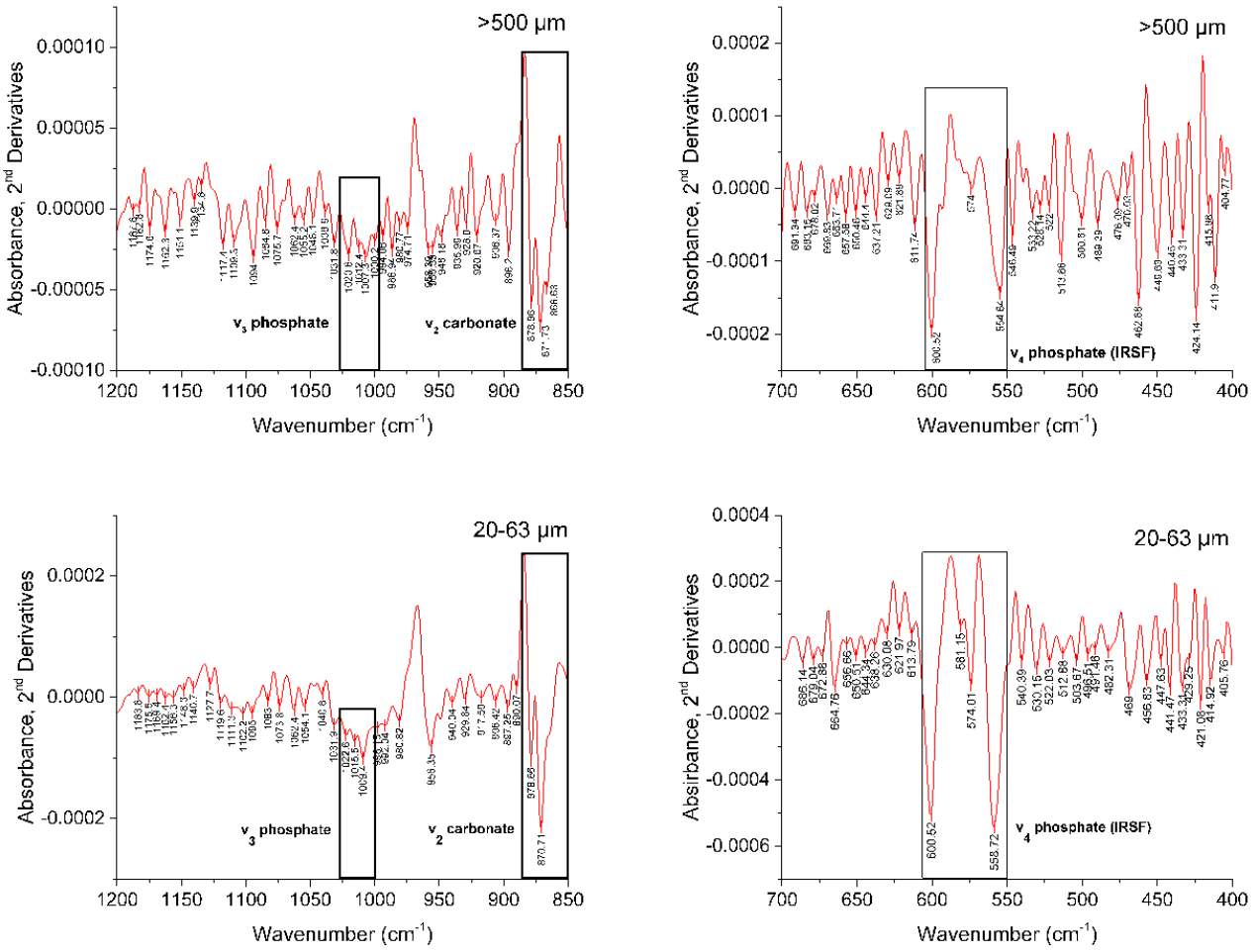

Figure 8. Example of 2nd derivative spectra of the v_4 PO_4^{3-} asymmetric bending vibrations in the region of 400-700 cm^{-1} (right column) and v_3 PO_4^{3-} asymmetric stretching modes at around 1010 cm^{-1} (left column) at different particle sizes for modern bovine mesosteal bone.

Regarding the number of the 2nd derivative components of the phosphate bands, they display a very small decrease with decreasing particle size, except at c. 1 µm particle size where a small increase is observed (Figure 8). Although the peak positions of the overlapping bands shift towards higher wavenumbers with decreasing particle size, this does not happen in a progressive manner or with a characteristic pattern. Additionally, the c. 630 cm^{-1} component, which is considered the vibration mode of OH, is observed in modern bone but shifts towards higher wavenumbers when crystallinity increases, due to diagenesis.

4. Conclusion

To summarize, we have shown in this study that particle size distribution leads to systematic changes in FTIR-ATR data as expressed by IRSF, C/P and Am/P indices. Specifically:

1. Removing the periosteal, endosteal and trabecular tissues prior to pulverization of mesosteal (mid-cortical) bone is necessary and eliminates uncertainties when using these semi-quantitative mid-IR indices for bone.
2. IRSF increases with decreasing particle sizes from >500 μm to 20-63 μm both in unheated and heated archaeological and modern bone samples. This is possibly an example of the Surovell and Stiner [26] "separation hypothesis" down to the 20-63 μm particle size, giving way to the "destruction hypothesis" when bone powder is consisted of particles of c. 1 μm, as there is a large decrease in IRSF values at this point.
3. The FWHM at c. 1010 cm^{-1} demonstrates a very strong inverse relationship with IRSF and a very strong linear relationship with particle size, decreasing with decreasing particle size from >500 μm to 20-63 μm. When bone powder consists of particles of c. 1 μm, the FWHM at c. 1010 cm^{-1} does not show any characteristic pattern and relationship with crystallinity, confirming that the boundaries between order and disorder in BAp crystals are still unclear. Overall, these patterns are strongly related to the changes that occur at the short- and long-range order of the BAp crystals during grinding.
4. C/P and Am/P follow an opposite relationship to IRSF, both decreasing from >500 μm to 20-63 μm particle size. When bone powder consists of particles of c. 1 μm, C/P and Am/P values vary with no characteristic patterns observed. The inverse relationship between IRSF and C/P also supports the effect of carbonate in the atomic order/disorder of BAp crystals.
5. The wavenumber of the main peaks and the 2nd derivative components of the bands in bone alter with decreasing particle size. The absence of the "labile" A_1 carbonate at 866 cm^{-1} in archaeological bone and its loss at lower particle sizes during grinding in modern bovine is noteworthy.
6. Absorbance of the IR radiation is strongly affected by the particle size, with higher absorbances for smaller bone powder particles. This observation indicates that for smaller particle sizes, there is a better contact between the sample and the prism, as well as a higher exposure of the bone powder's components to the IR light.

Therefore, we propose a standard preparation procedure for bone powder analysed using FTIR-ATR (Figure 9). This standard process should be followed to improve accuracy, consistency, reliability, reproducibility and comparability of the data for the systematic evaluation of bone in archaeological, anthropological, paleontological, forensic and biomedical studies:

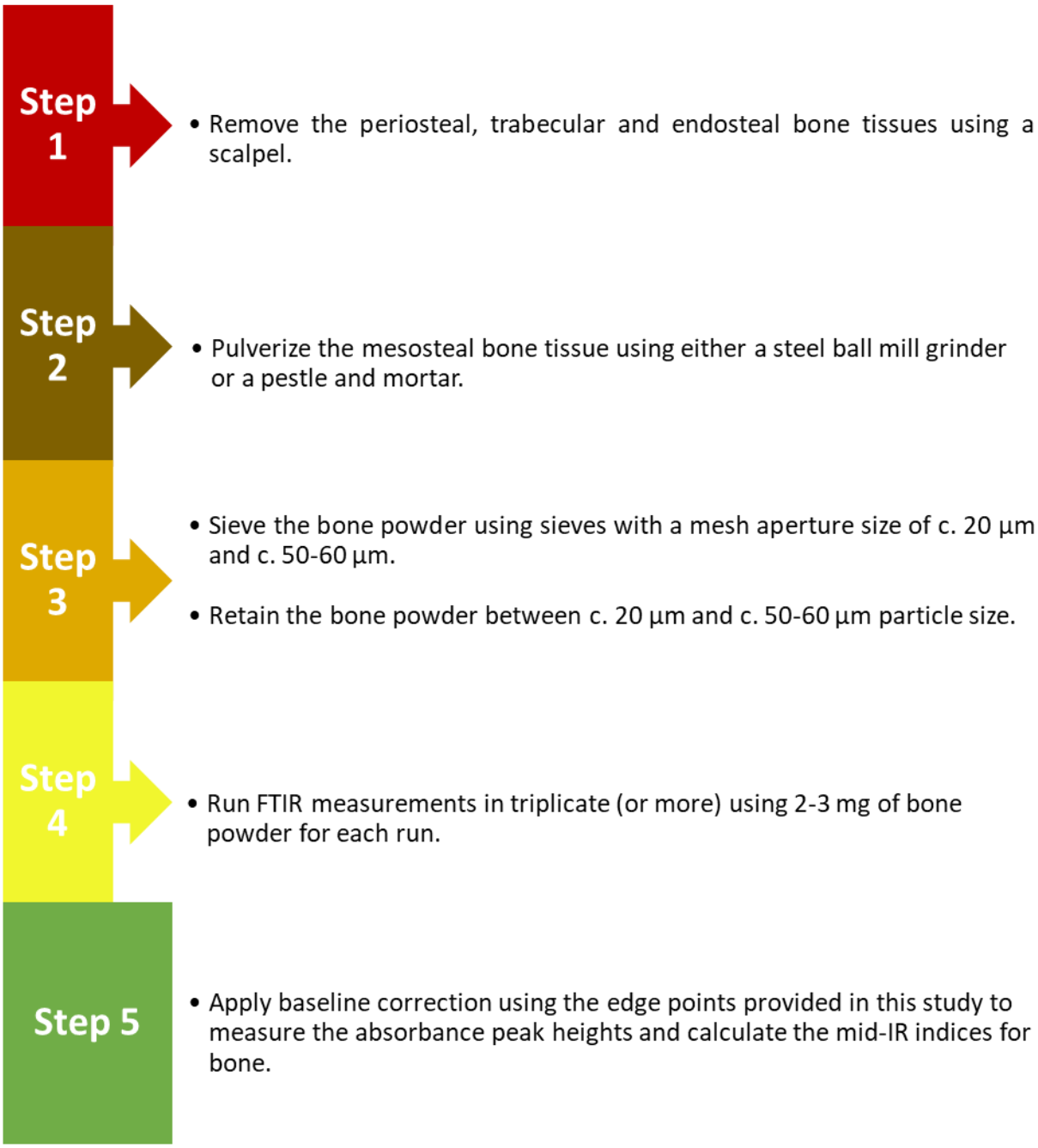

Figure 9. Sample preparation and analysis strategy for bone powder analysed using FTIR-ATR.

Acknowledgements

We are grateful to Dan Bradley, Adamantios Sampson, Morten Allentoft, Chaido Koukouli-Chrysanthaki, Ingrid Mainland, Jacqui Mulville, David Allen, Victoria Mullin, Georgios Kazantzis, Katrien Van de Vijver and Bart Robberechts, the Greek Ministry of Culture and Sports, the Ephorate of Palaeoanthropology and Speleology (Greece), the Ephorates of Antiquities in Boeotia and Serres (Greece), and the Archaeology department of the city council of Mechelen for giving us access to the material used in this study. We are also indebted to Peter Zioupos

for the two modern human samples (NHS REC approval 10/H0107/14) which were used as references with the kind permission of the Department of Biology Ethics Committee (BEC) of the University of York.
IK would like to thank Onassis Foundation (Grant no. F ZL 047-1/2015-2016), Leventis Foundation and the Greek Archaeological Committee UK (GACUK). SP would like to thank Brian Chait and the Laboratory of Mass Spectrometry and Gaseous Ion Chemistry (Rockefeller University) for use of the Retsch PM100 ball mill and useful help and support. KP thanks the Leverhulme Trust (PLP-2012-116) and MJC thanks the DNRF for the award of a Niels Bohr Professorship.

References

[1] S. Weiner, W. Traub, Organization of hydroxyapatite crystals within collagen fibrils, FEBS Lett. 206 (1986) 262–266. https://www.ncbi.nlm.nih.gov/pubmed/3019771.
[2] S. Weiner, H.D. Wagner, The material bone: Structure-mechanical function relations, Annu. Rev. Mater. Sci. 28 (1998) 271–298.
[3] A.L. Boskey, Bone mineral crystal size, Osteoporos. Int. 14 Suppl 5 (2003) S16–20; discussion S20–1. doi:10.1007/s00198-003-1468-2.
[4] B. Wopenka, J.D. Pasteris, A mineralogical perspective on the apatite in bone, Materials Science and Engineering: C. 25 (2005) 131–143. doi:10.1016/j.msec.2005.01.008.
[5] P. Zioupos, J.D. Currey, A. Casinos, Exploring the effects of hypermineralisation in bone tissue by using an extreme biological example, Connect. Tissue Res. 41 (2000) 229–248. https://www.ncbi.nlm.nih.gov/pubmed/11264871.
[6] P. Zioupos, C. Kaffy, J.D. Currey, Tissue heterogeneity, composite architecture and fractal dimension effects in the fracture of ageing human bone, Int. J. Fract. 139 (2006) 407–424. doi:10.1007/s10704-006-6581-8.
[7] J.S. Yerramshetty, O. Akkus, The associations between mineral crystallinity and the mechanical properties of human cortical bone, Bone. 42 (2008) 476–482. doi:10.1016/j.bone.2007.12.001.
[8] E.P. Paschalis, E. DiCarlo, F. Betts, P. Sherman, R. Mendelsohn, A.L. Boskey, FTIR microspectroscopic analysis of human osteonal bone, Calcif. Tissue Int. 59 (1996) 480–487. http://www.ncbi.nlm.nih.gov/pubmed/8939775.
[9] J.D. Pasteris, B. Wopenka, J.J. Freeman, K. Rogers, E. Valsami-Jones, J.A.M. van der Houwen, M.J. Silva, Lack of OH in nanocrystalline apatite as a function of degree of atomic order: implications for bone and biomaterials, Biomaterials. 25 (2004) 229–238. doi:10.1016/S0142-9612(03)00487-3.
[10] T. Leventouri, Synthetic and biological hydroxyapatites: crystal structure questions, Biomaterials. 27 (2006) 3339–3342. doi:10.1016/j.biomaterials.2006.02.021.
[11] C. Rey, C. Combes, C. Drouet, H. Sfihi, A. Barroug, Physico-chemical properties of nanocrystalline apatites: Implications for biominerals and biomaterials, Materials Science and Engineering: C. 27 (2007) 198–205. doi:10.1016/j.msec.2006.05.015.
[12] S. Gourion- Arsiquaud, J.C. Burket, Spatial variation in osteonal bone properties relative to tissue and animal age, Journal of Bone and Mineral Research. (2009). http://onlinelibrary.wiley.com/doi/10.1359/jbmr.090201/full.
[13] T. Sakae, H. Nakada, J.P. LeGeros, Historical Review of Biological Apatite Crystallography, J. Hard Tissue Biol. 24 (2015) 111–122. doi:10.2485/jhtb.24.111.
[14] H.C.W. Skinner, Mineralogy of Bones, in: O. Selinus (Ed.), Essentials of Medical Geology: Revised Edition, Springer Netherlands, Dordrecht, 2013: pp. 667–693. doi:10.1007/978-94-007-4375-5_30.
[15] D.R. Brothwell, A.M. Pollard, Handbook of archaeological sciences, anchecata.colmich.edu.mx, 2001. http://anchecata.colmich.edu.mx/janium/Tablas/tabla108546.pdf.
[16] T. Brown, K. Brown, Biomolecular archaeology An introduction, Wiley-blackwell, Sussex, 2011.
[17] C. Nielsen-Marsh, A. Gernaey, G. Turner-Walker, R. Hedges, A.W.G. Pike, M. Collins, The chemical degradation of bone, in: M. Cox, S. Mays (Eds.), Human Osteology: In Archaeology and Forensic Science, Cambridge University Press, 2000: pp. 439–454. http://eprints.soton.ac.uk/394456/ (accessed September 20, 2016).

[18] M.J. Collins, C.M. Nielsen-Marsh, J. Hiller, C.I. Smith, J.P. Roberts, R.V. Prigodich, T.J. Wess, J. Csapo, A.R. Millard, G. Turner-Walker, The survival of organic matter in bone: a review, Archaeometry. 44 (2002) 383–394.
[19] J. Lee–Thorp, Two decades of progress towards understanding fossilization processes and isotopic signals in calcified tissue minerals, Archaeometry. 44 (2002) 435–446. doi:10.1111/1475-4754.t01-1-00076.
[20] S.W. Keenan, From bone to fossil: A review of the diagenesis of bioapatite, Am. Mineral. 101 (2016) 1943–1951. doi:10.2138/am-2016-5737.
[21] C. Kendall, A.M.H. Eriksen, I. Kontopoulos, M.J. Collins, G. Turner-Walker, Diagenesis of archaeological bone and tooth, Palaeogeogr. Palaeoclimatol. Palaeoecol. 491 (2018) 21–37. doi:10.1016/j.palaeo.2017.11.041.
[22] S. Weiner, O. Bar-Yosef, States of preservation of bones from prehistoric sites in the Near East: A survey, J. Archaeol. Sci. 17 (1990) 187–196. doi:10.1016/0305-4403(90)90058-D.
[23] M.C. Stiner, S.L. Kuhn, S. Weiner, O. Bar-Yosef, Differential burning, recrystallization, and fragmentation of archaeological bone, J. Archaeol. Sci. 22 (1995) 223–237.
[24] A. Sillen, J. Parkington, Diagenesis of Bones from Eland's Bay Cave, J. Archaeol. Sci. 23 (1996) 535–542. doi:10.1006/jasc.1996.0050.
[25] L.E. Wright, H.P. Schwarcz, Infrared and Isotopic Evidence for Diagenesis of Bone Apatite at Dos Pilas, Guatemala: Palaeodietary Implications, J. Archaeol. Sci. 23 (1996) 933–944.
[26] T.A. Surovell, M.C. Stiner, Standardizing Infra-red Measures of Bone Mineral Crystallinity: an Experimental Approach, J. Archaeol. Sci. 28 (2001) 633–642. doi:10.1006/jasc.2000.0633.
[27] M.C. Stiner, S.L. Kuhn, T.A. Surovell, P. Goldberg, L. Meignen, S. Weiner, O. Bar-Yosef, Bone Preservation in Hayonim Cave (Israel): a Macroscopic and Mineralogical Study, J. Archaeol. Sci. 28 (2001) 643–659. doi:10.1006/jasc.2000.0634.
[28] I. Reiche, C. Vignaud, M. Menu, The crystallinity of ancient bone and dentine: new insights by transmission electron microscopy, Archaeometry. 44 (2002) 447–459. doi:10.1111/1475-4754.00077.
[29] C.N.G. Trueman, A.K. Behrensmeyer, N. Tuross, S. Weiner, Mineralogical and compositional changes in bones exposed on soil surfaces in Amboseli National Park, Kenya: diagenetic mechanisms and the role of sediment pore fluids, J. Archaeol. Sci. 31 (2004) 721–739. doi:10.1016/j.jas.2003.11.003.
[30] E.T. Stathopoulou, V. Psycharis, G.D. Chryssikos, V. Gionis, G. Theodorou, Bone diagenesis: New data from infrared spectroscopy and X-ray diffraction, Palaeogeogr. Palaeoclimatol. Palaeoecol. 266 (2008) 168–174. doi:10.1016/j.palaeo.2008.03.022.
[31] C.N. Trueman, K. Privat, J. Field, Why do crystallinity values fail to predict the extent of diagenetic alteration of bone mineral?, Palaeogeogr. Palaeoclimatol. Palaeoecol. 266 (2008a) 160–167. doi:10.1016/j.palaeo.2008.03.038.
[32] F. Brock, T. Higham, C.B. Ramsey, Pre-screening techniques for identification of samples suitable for radiocarbon dating of poorly preserved bones, J. Archaeol. Sci. 37 (2010) 855–865. doi:10.1016/j.jas.2009.11.015.
[33] G. Piga, A. Santos-Cubedo, A. Brunetti, M. Piccinini, A. Malgosa, E. Napolitano, S. Enzo, A multi-technique approach by XRD, XRF, FT-IR to characterize the diagenesis of dinosaur bones from Spain, Palaeogeogr. Palaeoclimatol. Palaeoecol. 310 (2011) 92–107. doi:10.1016/j.palaeo.2011.05.018.
[34] H.I. Hollund, F. Ariese, R. Fernandes, M.M.E. Jans, H. Kars, Testing an alternative high-throughput tool for investigating bone diagenesis: FTIR in Attenuated Total Reflection (ATR) mode, Archaeometry. 55 (2013) 507–532. doi:10.1111/j.1475-4754.2012.00695.x.
[35] T.J.U. Thompson, M. Gauthier, M. Islam, The application of a new method of Fourier Transform Infrared Spectroscopy to the analysis of burned bone, J. Archaeol. Sci. 36 (2009) 910–914. doi:10.1016/j.jas.2008.11.013.
[36] M.M. Beasley, E.J. Bartelink, L. Taylor, R.M. Miller, Comparison of transmission FTIR, ATR, and DRIFT spectra: implications for assessment of bone bioapatite diagenesis, J. Archaeol. Sci. 46 (2014) 16–22. doi:10.1016/j.jas.2014.03.008.
[37] J.A. Lee-Thorp, N.J. van der Merwe, Aspects of the chemistry of modern and fossil biological apatites, J. Archaeol. Sci. 18 (1991) 343–354. doi:10.1016/0305-4403(91)90070-6.

[38] M. Sponheimer, J.A. Lee-Thorp, Alteration of Enamel Carbonate Environments during Fossilization, J. Archaeol. Sci. 26 (1999) 143–150. doi:10.1006/jasc.1998.0293.
[39] G. Nagy, T. Lorand, Z. Patonai, G. Montsko, I. Bajnoczky, A. Marcsik, L. Mark, Analysis of pathological and non-pathological human skeletal remains by FT-IR spectroscopy, Forensic Sci. Int. 175 (2008) 55–60. doi:10.1016/j.forsciint.2007.05.008.
[40] C. Chadefaux, A.-S. Le Hô, L. Bellot-Gurlet, I. Reiche, Curve-fitting micro-ATR-FTIR studies of the Amide I and II bands of type I collagen in archaeological bone materials, E-PS. 6 (2009) 129–137.
[41] K.E. Squires, T.J.U. Thompson, M. Islam, A. Chamberlain, The application of histomorphometry and Fourier Transform Infrared Spectroscopy to the analysis of early Anglo-Saxon burned bone, J. Archaeol. Sci. 38 (2011) 2399–2409. doi:10.1016/j.jas.2011.04.025.
[42] J.D. Fredericks, P. Bennett, A. Williams, K.D. Rogers, FTIR spectroscopy: a new diagnostic tool to aid DNA analysis from heated bone, Forensic Sci. Int. Genet. 6 (2012) 375–380.
[43] G. Piga, D. Gonçalves, T.J.U. Thompson, A. Brunetti, A. Malgosa, S. Enzo, Understanding the Crystallinity Indices Behavior of Burned Bones and Teeth by ATR-IR and XRD in the Presence of Bioapatite Mixed with Other Phosphate and Carbonate Phases, International Journal of Spectroscopy. 2016 (2016). doi:10.1155/2016/4810149.
[44] G. Dal Sasso, M. Lebon, I. Angelini, L. Maritan, D. Usai, G. Artioli, Bone diagenesis variability among multiple burial phases at Al Khiday (Sudan) investigated by ATR-FTIR spectroscopy, Palaeogeogr. Palaeoclimatol. Palaeoecol. 463 (2016) 168–179. doi:10.1016/j.palaeo.2016.10.005.
[45] J.D. Termine, A.S. Posner, Infra-Red Determination of the Percentage of Crystallinity in Apatitic Calcium Phosphates, Nature. 211 (1966) 268–270. doi:10.1038/211268a0.
[46] Y. Asscher, L. Regev, S. Weiner, E. Boaretto, Atomic Disorder in Fossil Tooth and Bone Mineral: An FTIR Study Using the Grinding Curve Method, Archeosciences. (2011) 135–141. doi:10.4000/archeosciences.3062.
[47] Y. Asscher, S. Weiner, E. Boaretto, Variations in Atomic Disorder in Biogenic Carbonate Hydroxyapatite Using the Infrared Spectrum Grinding Curve Method, Adv. Funct. Mater. 21 (2011) 3308–3313. doi:10.1002/adfm.201100266.
[48] T.J.U. Thompson, M. Islam, K. Piduru, A. Marcel, An investigation into the internal and external variables acting on crystallinity index using Fourier Transform Infrared Spectroscopy on unaltered and burned bone, Palaeogeogr. Palaeoclimatol. Palaeoecol. 299 (2011) 168–174. doi:10.1016/j.palaeo.2010.10.044.
[49] C. Snoeck, J. Lee-Thorp, R.J. Schulting, From bone to ash: compositional and structural changes in burned modern and archaeological bone, Palaeogeogr. Palaeoclimatol. Palaeoecol. 416 (2014) 55–68.
[50] C.N. Trueman, Chemical taphonomy of biomineralized tissues, Palaeontology. 56 (2013) 475–486. doi:10.1111/pala.12041.
[51] F.D. Pate, J.T. Hutton, K. Norrish, Ionic exchange between soil solution and bone: toward a predictive model, Appl. Geochem. 4 (1989) 303–316.
[52] R.Z. LeGeros, Effect of Carbonate on the Lattice Parameters of Apatite, Nature. 206 (1965) 403. doi:10.1038/206403a0.
[53] R.Z. LeGeros, O.R. Trautz, J.P. LeGeros, E. Klein, W.P. Shirra, Apatite crystallites: effects of carbonate on morphology, Science. 155 (1967) 1409–1411. doi:10.1126/science.155.3768.1409.
[54] R.Z. LeGeros, O.R. Trautz, E. Klein, J.P. LeGeros, Two types of carbonate substitution in the apatite structure, Experientia. 25 (1969) 5–7. doi:10.1007/BF01903856.
[55] R.Z. LeGeros, Apatites in biological systems, Prog. Cryst. Growth Charact. Mater. 4 (1981) 1–45.
[56] J.C. Elliott, D.W. Holcomb, R.A. Young, Infrared determination of the degree of substitution of hydroxyl by carbonate ions in human dental enamel, Calcif. Tissue Int. 37 (1985) 372–375. https://www.ncbi.nlm.nih.gov/pubmed/3930033.
[57] C. Rey, B. Collins, T. Goehl, I.R. Dickson, M.J. Glimcher, The carbonate environment in bone mineral: a resolution-enhanced Fourier Transform Infrared Spectroscopy Study, Calcif. Tissue Int. 45 (1989) 157–164. https://www.ncbi.nlm.nih.gov/pubmed/2505907.
[58] E. Pucéat, B. Reynard, C. Lécuyer, Can crystallinity be used to determine the degree of chemical alteration of biogenic apatites?, Chem. Geol. 205 (2004) 83–97. doi:10.1016/j.chemgeo.2003.12.014.
[59] M.E. Fleet, X. Liu, Location of type B carbonate ion in type A–B carbonate apatite synthesized at

high pressure, J. Solid State Chem. 177 (2004) 3174–3182. doi:10.1016/j.jssc.2004.04.002.
[60] C.N. Trueman, M.R. Palmer, J. Field, K. Privat, N. Ludgate, V. Chavagnac, D.A. Eberth, R. Cifelli, R.R. Rogers, Comparing rates of recrystallisation and the potential for preservation of biomolecules from the distribution of trace elements in fossil bones, C. R. Palevol. 7 (2008b) 145–158. doi:10.1016/j.crpv.2008.02.006.
[61] A. Antonakos, E. Liarokapis, T. Leventouri, Micro-Raman and FTIR studies of synthetic and natural apatites, Biomaterials. 28 (2007) 3043–3054. doi:10.1016/j.biomaterials.2007.02.028.
[62] M. Lebon, I. Reiche, J.-J. Bahain, C. Chadefaux, A.-M. Moigne, F. Fröhlich, F. Sémah, H.P. Schwarcz, C. Falguères, New parameters for the characterization of diagenetic alterations and heat-induced changes of fossil bone mineral using Fourier transform infrared spectrometry, J. Archaeol. Sci. 37 (2010) 2265–2276. doi:10.1016/j.jas.2010.03.024.
[63] C.L. King, N. Tayles, K.C. Gordon, Re-examining the chemical evaluation of diagenesis in human bone apatite, J. Archaeol. Sci. 38 (2011) 2222–2230. doi:10.1016/j.jas.2011.03.023.
[64] T.J.U. Thompson, M. Islam, M. Bonniere, A new statistical approach for determining the crystallinity of heat-altered bone mineral from FTIR spectra, J. Archaeol. Sci. 40 (2013) 416–422. doi:10.1016/j.jas.2012.07.008.
[65] L. Regev, K.M. Poduska, L. Addadi, S. Weiner, E. Boaretto, Distinguishing between calcites formed by different mechanisms using infrared spectrometry: archaeological applications, J. Archaeol. Sci. 37 (2010) 3022–3029. doi:10.1016/j.jas.2010.06.027.
[66] K.M. Poduska, L. Regev, E. Boaretto, L. Addadi, S. Weiner, L. Kronik, S. Curtarolo, Decoupling local disorder and optical effects in infrared spectra: differentiating between calcites with different origins, Adv. Mater. 23 (2011) 550–554. doi:10.1002/adma.201003890.
[67] M.J. Collins, P. Galley, Towards an optimal method of archaeological collagen extraction: the influence of pH and grinding, Anc. Biomol. 2 (1998) 209–223.
[68] C.J. Adler, W. Haak, D. Donlon, A. Cooper, Survival and recovery of DNA from ancient teeth and bones, J. Archaeol. Sci. 38 (2011) 956–964. doi:10.1016/j.jas.2010.11.010.
[69] F.D. Pate, J.T. Hutton, The use of soil chemistry data to address post-mortem diagenesis in bone mineral, J. Archaeol. Sci. 15 (1988) 729–739.
[70] P. Karkanas, O. Bar-Yosef, P. Goldberg, S. Weiner, Diagenesis in Prehistoric Caves: the Use of Minerals that Form In Situ to Assess the Completeness of the Archaeological Record, J. Archaeol. Sci. 27 (2000) 915–929. doi:10.1006/jasc.1999.0506.
[71] L. Wilson, A.M. Pollard, Here today, gone tomorrow? integrated experimentation and geochemical modeling in studies of archaeological diagenetic change, Acc. Chem. Res. 35 (2002) 644–651. doi:10.1021/ar000203s.
[72] H. Ou-Yang, E.P. Paschalis, W.E. Mayo, A.L. Boskey, R. Mendelsohn, Infrared Microscopic Imaging of Bone: Spatial Distribution of CO32−, J. Bone Miner. Res. 16 (2001) 893–900. doi:10.1359/jbmr.2001.16.5.893.
[73] P. Kristova, K.J. Rutt, L.J. Hopkinson, The effect of the particle size on the fundamental vibrations of the [CO32-] anion in calcite, J. Phys. Chem. A. 119 (2015) 4891–4897. doi:10.1021/acs.jpca.5b02942.
[74] B. Udvardi, I.J. Kovács, T. Fancsik, P. Kónya, M. Bátori, F. Stercel, G. Falus, Z. Szalai, Effects of Particle Size on the Attenuated Total Reflection Spectrum of Minerals, Appl. Spectrosc. 71 (2017) 1157–1168. doi:10.1177/0003702816670914.
[75] C. Rey, C. Combes, What bridges mineral platelets of bone?, Bonekey Rep. 3 (2014) 586. doi:10.1038/bonekey.2014.81.
[76] Y. Wang, S. Von Euw, F.M. Fernandes, S. Cassaignon, M. Selmane, G. Laurent, G. Pehau-Arnaudet, C. Coelho, L. Bonhomme-Coury, M.-M. Giraud-Guille, F. Babonneau, T. Azaïs, N. Nassif, Water-mediated structuring of bone apatite, Nat. Mater. 12 (2013) 1144–1153. doi:10.1038/nmat3787.
[77] H. Tong, P. Tan, N. Xu, From Crystals to Disordered Crystals: A Hidden Order-Disorder Transition, Sci. Rep. 5 (2015) 15378. doi:10.1038/srep15378.
[78] J. Aufort, L. Ségalen, C. Gervais, C. Brouder, E. Balan, Modeling the attenuated total reflectance infrared (ATR-FTIR) spectrum of apatite, Phys. Chem. Miner. 43 (2016) 615–626. doi:10.1007/s00269-016-0821-x.
[79] M.E. Fleet, X. Liu, P.L. King, Accommodation of the carbonate ion in apatite: An FTIR and X-ray

structure study of crystals synthesized at 2–4 GPa, Am. Mineral. 89 (2004) 1422–1432. doi:10.2138/am-2004-1009.
[80] M.E. Fleet, Infrared spectra of carbonate apatites: v2-Region bands, Biomaterials. 30 (2009) 1473–1481. doi:10.1016/j.biomaterials.2008.12.007.